Journal of Biomolecular NMR, **20:** 333–349, 2001.
KLUWER/ESCOM

Modeling the dynamics of a mutated stem-loop in the SL1 domain of HIV-1_{Lai} genomic RNA by ^{1}H-NOESY spectra

Simone Fausti[a,b], Giovanni La Penna[a], Jacques Paoletti[c], Daniel Genest[c], Gérard Lancelot[c] & Angelo Perico[a,*]

[a]*Istituto di Studi Chimico fisici di macromolecole Sintetiche e Naturali, National Research Council (CNR), Via De Marini 6, I-16149 Genova, Italy;* [b]*Dipartimento di Chimica e Chimica Industriale, Università di Genova, Via Dodecaneso 31, I-16146 Genova, Italy;* [c]*Centre de Biophysique Moleculaire, UPR 4301 CNRS, Affiliated to the University of Orléans, Rue Charles Sadron, F-45071 Orléans Cedex 2, France*

Received 12 February 2001; Accepted 18 May 2001

Key words: dynamics, HIV, NOESY, RNA

Abstract

The cross-peaks of ^{1}H-NOESY spectra at different time delays are compared to a mode-coupling diffusion (MCD) calculation, including the evaluation of the full ^{1}H relaxation matrix, in the case of a 23 nucleotide fragment of the stem-loop SL1 domain of HIV-1_{Lai} genomic RNA mutated in a single position. The MCD theory gives significant agreement with ^{1}H relaxation experiments enabling a thorough understanding of the differential local dynamics along the sequence and particularly of the dynamics of nucleotides in the stem and in the loop. The differential dynamics of this hairpin structure is important in directing the dimerization of the retroviral genome, a fundamental step in the infectious process. The demonstration of a reliable use of time dependent NOE cross-peaks, largely available from NMR solution structure determination, coupled to MCD analysis, to probe the local dynamics of biological macromolecules, is a result of general interest of this paper.

Introduction

Dynamic processes may be important in determining the biological function of biopolymers. A typical case is shown by the RNA molecule studied in this work. This molecule is the SL1 domain of the RNA genome in the HIV-1_{Lai} retrovirus which is uniquely required for efficient dimerization, a crucial point in the infectious process (Laughrea and Jetté, 1994; Marquet et al., 1994; Paillart et al., 1994; Skripkin et al., 1994; Girard et al., 1995; Muriaux et al., 1995, 1996). This domain has the form of a hairpin, characterized by a highly conserved sequence which is organized in a stem-loop structure. Dimerization is initiated when two SL1 domains of two strands interact by base pairing to form a kissing-loop which then isomerizes into a more stable linear duplex (Mujeeb et al., 1998; Girard et al., 1999; Theilleux-Delalande et al., 2000). In the formation of the kissing-loop, it appears that the two flexible loops have a critical role because they allow pairing of the two complementary loop sequences, while the stem duplexes remain the same. In order to study the dynamic properties of the SL1 stem-loop, the nucleotide G12 has been mutated into A12, to prevent the spontaneous dimerization process of the oligonucleotide and to keep the purine character of the base (Kieken et al., in preparation).

Among the several techniques available to probe local dynamics and flexibility of biological macromolecules, NMR relaxation on different nuclei along the sequence is the most important and universal technique. Usually, T_1, T_2 and NOE experiments on ^{13}C and ^{15}N nuclei are performed. The data acquired by these experiments, which generally require the enrichment of the sample, are collected independently from the main effort of determining the solution structure.

*To whom correspondence should be addressed. E-mail: perico@imag.ge.cnr.it

Alternatively, or in addition, one can use ^{1}H-NOESY spectra, normally available from the solution structure determination (Macura and Ernst, 1980; Wüthrich, 1986; Forster, 1991; Cavanagh, 1996). These data may give local information on the dynamics of H-H distance vectors via the contribution of all the H-H pairs in the relaxation matrix. Normally, this information is analyzed using empirical estimations of the numerous time correlation functions involved and thus increasing, for such an extensive interacting system, the difficulties in obtaining a reliable understanding of the physics involved. Two classes of approaches have been used to investigate local dynamics from NMR relaxation processes. In the first class, simple (Lipari and Szabo, 1982; Clore et al., 1990) and more advanced (Tugarinov et al., 2001) fitting models of the diffusive rotational and/or jump process are assumed and a limited set of diffusive properties (diffusion constants, reciprocal frames orientation and mean-field parameters affecting these orientations) are identified. The calculated data are then optimized by varying these parameters to have the best agreement with experiments. The second class of analysis consists in calculating the NMR dynamical quantities by assuming a model of the interactions between the macromolecule's constituent particles: again, both direct calculation of local order parameters through computer simulations (Withka et al., 1991; Prompers et al., 2001) or by normal-mode based analysis (Prompers and Brüschweiler, 2000) require some hypothesis about the 'decoupling' of overall rotation and internal motions. It is, therefore, important to develop universal molecular approaches of the second class to the internuclear vectors dynamics that avoid both the approximation of separation between time-scales in the dynamics and the use of empirical parameters that are typical of fitting procedures.

Such a theoretical approach was recently developed by using a mode-coupling solution to the diffusion equation (Perico and Pratolongo, 1997; La Penna et al., 1999b) describing the time evolution of fluctuating biological structures. This approach uses statistical averages evaluated by atomistic Molecular Dynamics (MD) or Monte Carlo simulations (Fausti et al., 1999; La Penna et al., 1999a, 2000a). The MD simulation algorithm applied to the macromolecule in the explicit water solvent with a few counterions has became widely used for biopolymers because of its ability to allow reasonable fluctuations of geometrical variables around structures obtained by X-ray or NMR. In this approach the local dynamics of a biological macromolecule, as probed by NMR techniques, are described as the rotational diffusion of a fluctuating structure, with the fluctuations estimated by molecular simulations.

The results obtained by using MD computed averages in diffusion theory agree in good measure to the T_1 experiments on ^{13}C and ^{15}N nuclei of small DNA duplexes (Fausti et al., 1999, 2000; La Penna et al., 2000b) and proteins (La Penna et al., 1999a, 2000a; Fausti et al., 2000). In this paper we apply for the first time this theoretical approach to compute all the H-H 2-rank time correlation functions and therefore the full relaxation matrix that governs the NOESY cross-peak intensities. We apply this approach to a 23 nucleotide fragment corresponding to the G12→A12 mutated SL1 stem-loop, whose solution structure has been recently determined (Kieken et al., in preparation). Finally, we compare experimental and calculated cross-peaks (hereafter abbreviated as CPs) for selected H-H pairs along the nucleotide sequence both in the stem and in the loop. In conclusion, the important properties of flexibility and dynamics of the studied fragment are discussed.

Materials and ^{1}H-NOESY cross-peaks

The ribooligonucleotide r(CUUGCUGAAGCACGCA CGGCAAG) was obtained by automated synthesis (Kieken et al., in preparation). NMR experiments were carried out on an AMX-500 spectrometer operating at 11.74 Tesla and processed on a X32 computer. NOESY spectra were performed on a 2 mM degassed and sealed sample. We used here the sequential assignment already proposed (Kieken et al., in preparation). A delay of 4 s was used in order to optimize the signal-to-noise ratio of the NOESY spectra without noticeable difference in the spin-state magnetization of the different protons. The t_1 data were zero-filled to 2048 points and processed with a sine 90° phase shifted function. This light apodization function did not distort the signal intensity and the resulting peaks had no truncation effect. Correct phasing of the data in both directions was achieved with great care in order to quench the zero-quantum contribution in the cross-peak integration.

Each cross-peak value was obtained by dividing the volume of the cross-peak by the volume of the corresponding diagonal peak (H5 for the H5-H6 NOE and H1′ for the H1′-H6/8 pairs) obtained at zero mixing time. Since some of the H5 resonances were over-

lapped with the H1′ resonances, the volume measured for each of the five unoverlapped H5 was compared with the average value computed by dividing the total volume of the diagonal containing all the H5 and H1′ resonances (between 5.0 and 6.1 ppm) by the corresponding number of protons (23H1′ plus 10H5). This average value was used for all the H5 or H1′ protons since no significant deviations were observed between the measured values.

The cross-peak volumes were calculated with integration routines of the UXNMR software package (Bruker Spectrospin). The errors on CPs have been computed as 10% for all the values larger than 0.005; for the smaller CPs we have used an absolute error of 0.001.

We conclude defining the CP names used in the sections concerning analysis and discussion:

- 'H5-H6 *intra*' indicates the CP between H5 and H6 on the same pyrimidine;
- 'H1′-H6/8 *intra*' refers to the CP between H1′ and H6 (in pyrimidines) or H8 (in purines), the protons belonging to the same nucleotide;
- 'H1′-H6/8 *inter*' indicates an analogous CP as above, but in this case H1′ belongs to the 5′ previous nucleotide in the sequence.

The relaxation matrix and the NOESY spectrum

In the ^{1}H-NOESY experiment (Jeener et al., 1979; Meier and Ernst, 1979; Sanders and Hunter, 1993; Cavanagh, 1996) on the RNA fragment, in theory, the transient NOE effects between all the ^{1}H couples are observed. If there are g groups (G_k, $k = 1, ..., g$) of equivalent nuclei where each G_k has n_k spins with Larmor frequency ω_k, the time evolution of the magnetization is described by the Solomon equations (Solomon, 1955). In turn, the matrix elements of the NOESY CPs evaluated at a mixing time t are given as (Macura and Ernst, 1980; Forster, 1991; Neuhaus and Williamson, 1989; Boelens et al., 1989):

$$O_{hk}(t) = \left[\exp(-\mathbf{R}t)\right]_{hk} = \sum_a V_{ha} \exp(-m_a t)\, V_{ak}^{-\mathbf{1}} \quad (h, k = 1, ..., g;\ h \neq k) \tag{1}$$

with $\mathbf{R}$ the relaxation matrix, describing the transfer of the magnetization between different groups, inside each group and with the environment; m_a and V_{ha} are the eigenvalues and eigenvectors of $\mathbf{R}$, respectively. The elements of the relaxation matrix are given in terms of the transition probabilities by (Macura and Ernst, 1980):

$$R_{hk} = \frac{1}{n_k}\sum_{i,j}\left[W_{ij}^{(2)} - W_{ij}^{(0)}\right] \quad i \in G_h \text{ and } j \in G_k \tag{2}$$

for the transfer of the magnetization from a spin in the group G_h to a spin in a different group G_k, and

$$R_{kk} = R_k^{\text{int}} + R_k^{\text{out}} + R_k^{(1)} \simeq R_k^{\text{int}} + R_k^{\text{out}} \tag{3}$$

for the diagonal terms, where R_k^{int} represents the transitions in the group G_k:

$$R_k^{\text{int}} = \frac{2}{n_k}\sum_{i<j}\left[W_{ij}^{(1)} + W_{ij}^{(2)}\right] \quad i, j \in G_k; \tag{4}$$

R_k^{out} the transfer of excitation between spins in G_k and spins in the other groups:

$$R_k^{\text{out}} = \frac{1}{n_k}\sum_{i,j}\left[W_{ij}^{(0)} + 2W_{ij}^{(1)} + W_{ij}^{(2)}\right] \quad i \in G_k \text{ and } j \notin G_k; \tag{5}$$

and $R_k^{(1)}$ represents the transfer of excitation from G_k spins to the environment. Note that this last term can be ignored at short mixing times, as in the second equality in Equation 3.

Finally, the a quanta transition probabilities $W_{ij}^{(a)}$, relative to dipolar coupling between nucleus i and nucleus j, are given in terms of spectral densities (Macura and Ernst, 1980; Cavanagh et al., 1996):

$$W_{ij}^{(0)} = q_{ij} J_{ij}\left(\omega_i - \omega_j\right); \quad W_{ij}^{(1)} = \frac{3}{2} q_{ij} J_{ij}\left(\omega_i\right); \quad W_{ij}^{(2)} = 6 q_{ij} J_{ij}\left(\omega_i + \omega_j\right) \tag{6}$$

with

$$q_{ij} = \frac{1}{20}\left(\frac{\gamma_i \gamma_j}{4\pi\varepsilon_0 c^2}\right)^2 \tag{7}$$

and $J_{ij}(\omega)$ the spectral density defined below (Equations 21 and 26) relative to 2-rank time correlation functions (TCFs) of the vector $\mathbf{r}_{ij}$ joining proton i and proton j.

The $W_{ij}^{(a)}$ elements of Equation 6 may become irrelevant for many of the proton couples due to the r_{ij} dependence, motivating the use of reduced relaxation matrices that involve only hydrogens in a certain averaged distance.

In the case that the spin system can be divided in only two groups of equivalent spins ($g = 2$), the

Solomon equations can be solved in analytical form giving the single CP:

$$\begin{aligned} O_{12}(t) &= \frac{R_{12}}{\Delta} \cdot \exp(-\sigma \cdot t) \cdot \sinh(\Delta \cdot t) \\ \sigma &= \frac{R_{11} + R_{22}}{2}; \\ \Delta &= \sqrt{\left(\frac{R_{11} - R_{22}}{2}\right)^2 + R_{12}R_{21}}. \end{aligned} \tag{8}$$

Between the extreme cases of the full relaxation matrix and the simple case of only two non equivalent groups of spins, many intermediate selections of the interacting spins can be adopted in order to reduce the number of H-H relaxations only to the important ones (this point will be discussed below).

Diffusion approach to the calculation of the H-H vector orientational dynamics

Given the equations of the previous section, relating the observables in the experiment to the 2-rank TCFs describing the relaxation of the H-H vectors, we can finally introduce a molecular description of these relaxations.

This is accomplished here by adopting, for the first time, the mode-coupling diffusion theory of the dynamics of a biological macromolecule to the computation of the relaxation matrix and the CP of ^{1}H-NOESY spectrum.

The diffusion theory treats the solvent hydrodynamically and adopts a detailed molecular model for the polymer in terms of beads (atoms or group of atoms) connected by real or virtual bonds diffusing in a atomistic potential. In the mode-coupling matrix representationion of the diffusion equation, the potential has no particular role, but is contained in the statistical averages necessary to the theory. The beads are represented as points in position $\mathbf{r}_i$, characterized by their friction coefficients $\zeta_i = 6\pi\eta a_i$, with η the solvent viscosity. The Stokes' radii a_i were calculated here by using the ASA method (Pastor and Karplus, 1988) with a zero probe radius by summing the surfaces of each group constituent, according to the procedure outlined in the literature (La Penna et al., 2000b). The main polymer model uses four and three beads for each purinic and pyrimidinic nucleotide (Table 1). This model, together with more detailed ones, will be described below.

Now, we briefly summarize the mode-coupling diffusion approach to describe the dynamics in polymer solutions (Perico and Pratolongo, 1997; La Penna et al., 1999b). Given a polymer of N_a beads of friction coefficients ζ_i and coordinates $\mathbf{r}_i$, $i = 1, \ldots, N_a$, connected by N_b bonds ($\mathbf{l}_i, i = 1, \ldots, N_b$) the macromolecule dynamics, described by the variables $\mathbf{l}_i$, is governed by the operator L, adjoint to the diffusion Smoluchowski operator D:

$$\frac{\partial \mathbf{l}}{\partial t} = L\mathbf{l}; \quad L = \sum_{i,j=1}^{N_a} \left[\nabla_i \cdot \mathbf{D}_{i,j} \cdot \nabla_j - (\nabla_i U / k_B T) \cdot \mathbf{D}_{i,j} \cdot \nabla_j\right] \tag{9}$$

where $\mathbf{D}_{i,j}$ is the diffusion tensor to be defined below, U is the potential energy of the beads as a function of the bead coordinates, k_B is the Boltzmann constant and T is the absolute temperature.

By expanding the conditional probability (solution to the Smoluchowski equation) in a complete set of eigenfunctions of L, the time autocorrelation function (TCF) of any coordinate-dependent dynamic variable with zero average $f(t)$, may be expressed in the standard form

$$\langle f(t)\ f(0)\rangle = \sum_i \langle f \mid \psi_i\rangle\langle\psi_i \mid f\rangle \exp(-\lambda_i t), \tag{10}$$

where $-\lambda_i$ and ψ_i are the eigenvalues and the normalized eigenfunctions of the operator L:

$$L\psi_i = -\lambda_i \psi_i. \tag{11}$$

By representing ψ_i in a set of basis functions $\Phi = \{\phi_m, m = 1, \ldots, M\}$,

$$\psi_i = \sum_{m=1}^{M} C_{m,i}\phi_m, \tag{12}$$

the diffusion eigenvalue Equation 11) may be written in matrix form:

$$\mathbf{F}\,\mathbf{C} = \mathbf{S}\,\mathbf{C}\,\mathbf{\Lambda}, \tag{13}$$

with $\mathbf{\Lambda} = \{\Lambda_{ij}\}$ the diagonal matrix of the eigenvalues λ_m, $\mathbf{C}$ the eigenvector matrix of coefficients $C_{i,m}$, $\mathbf{S}$ the metric matrix

$$S_{ij} = \langle \phi_i \mid \phi_j \rangle \tag{14}$$

and $\mathbf{F}$ the equilibrium force matrix

$$\begin{aligned} F_{ij} &= -\langle \phi_i \mid L\phi_j \rangle \\ &= \sum_{m,n=1}^{N_a} \left\langle (\nabla_m \phi_i) \cdot \mathbf{D}_{mn} \cdot (\nabla_n \phi_j) \right\rangle. \end{aligned} \tag{15}$$

The diffusion tensor $\mathbf{D}$ is given by

Table 1. Bead models for the RNA molecule with Stokes' radii computed from Accessible Surface Area (atom names as in PDB standards)

Model		Atoms	Center	Radius (nm)
B	Backbone	5′-end: C5′, 1H5′, 2H5′, O5′, H5T	O5′	0.18
		C4′, H4′, O4′, C1', H1′, C2′, H2′, 1O2′, HO'2, C3′, H3′	C4′	0.25
		O3′, P, O1P, O2P, O5′, C5′, 1H5′, 2H5′	P	0.25
		3′-end: C4′, H4′, O4′, C1', H1′, C2′, 1H2′, O2′, HO'2, C3′, H3′, O3′, H3T	C4′	0.28
	Cytosine	N1, C2, O2, N3, C4, N4, 1H4, 2H4, C5, H5, C6, H6	N1	0.28
	Guanine	N9, C8, H8, N7, C5, C4	N9	0.19
		N3, C2, N2, 1H2, 2H2, N1, H1, C6, O6	N1	0.25
	Adenine	N9, C8, H8, N7, C5, C4	N9	0.19
		N3, C2, H2, N1, C6, N6, 1H6, 2H6	N1	0.24
	Uracil	N1, C2, O2, N3, H3, C4, O4, C5, H5, C6, H6	N1	0.28
B5	Backbone	5′-end: C5′, 1H5′, 2H5′, O5′, H5T	O5′	0.18
		C4′, H4′, O4′, C1', H1′, C2′, 1H2′, O2′, HO'2, C3′, H3′	C2′	0.25
		O3′, P, O1P, O2P, O5′	P	0.21
		C5′, 1H5′, 2H5′	C5′	0.13
		3′-end: C4′, H4′, O4′, C1', H1′, C2′, 1H2′, O2′, HO'2, C3′, H3′, O3′, H3T	C2′	0.28
	Bases	as in model B		
BH	Backbone	as in model B		
	Cytosine	9/10 of the surface area for the corresponding bead in model B	N1	0.27
		1/10 of the surface area for the corresponding bead in model B	H6	0.09
	Guanine	9/10 of the surface area for the bead centered in N9 in model B	N9	0.18
		1/10 of the surface area for the bead centered in N9 in model B	H8	0.06
		as in model B	N1	0.25
	Adenine	9/10 of the surface area for the bead centered in N9 in model B	N9	0.18
		1/10 of the surface area for the bead centered in N9 in model B	H8	0.06
		as in model B	N1	0.24
	Uracil	9/10 of the surface area for the corresponding bead in model B	N1	0.26
		1/10 of the surface area for the corresponding bead in model B	H6	0.09

$$\mathbf{D}_{ij} = D_i \mathbf{H}_{ij},$$

$$\mathbf{H}_{ij} = \mathbf{1}\delta_{ij} + \alpha\zeta_i \mathbf{T}_{ij}(1 - \delta_{ij}), \tag{16}$$

$$\mathbf{T}_{ij} \;=\; (8\pi\eta\, r_{ij})^{-1}\left[\mathbf{1} + \mathbf{r}_{ij}\mathbf{r}_{ij}/r_{ij}^2\right],$$

with $\mathbf{H}$ and $\mathbf{T}$ representing the hydrodynamic interaction matrix and Oseen tensor, respectively.

$$D_i = k_B T/\zeta_i \tag{17}$$

is the diffusion coefficient of each bead and η the solvent viscosity.

The factor α in the hydrodynamic interaction of Equation 16 is a parameter whose values are restricted to the range $0.5 < \alpha < 1.0$ so as to maintain a positive definite $\mathbf{H}$, while $\alpha = 1.0$ corresponds to the full interaction strength related to the specific choice of friction coefficients. In this work we used $\alpha = 0.7$ according to a recent choice for nucleic acids (La Penna et al., 2000b).

The ensemble equilibrium averages, indicated within angular brackets in the above equations, are calculated as

$$\begin{aligned}\langle a|b\rangle \;&=\; \int P_{eq}(\mathbf{r})a(\mathbf{r})\mathrm{d}\mathbf{r} \\ &=\; \int \exp(-U(\mathbf{r})/k_B T)a(\mathbf{r})b(\mathbf{r})\mathrm{d}\mathbf{r}/ \\ &\quad \int \exp(-U(\mathbf{r})/k_B T)\mathrm{d}\mathbf{r},\end{aligned} \tag{18}$$

with $P_{eq}(\mathbf{r})$ the equilibrium distribution function of bead coordinates and U the potential function in terms of the bead coordinates. In the following, the equi-

librium statistical averages will be calculated by time averaging along a MD trajectory for the full atomistic RNA fragment in explicit water (see next section). As the eigenfunctions ψ_i are orthonormalized, the coefficient matrix **C** should satisfy the normalization equation

$$(\mathbf{C}^T\mathbf{S}\mathbf{C})_{ij} \;=\; \langle \psi_i \psi_j \rangle = \delta_{ij}. \tag{19}$$

Accurate approximations to the TCFs evaluation are obtained by taking basis functions in the basis set built with increasing power of the variables, bond vectors or their linear combinations, in the spirit of the mode-coupling theory.

First and second order basis sets, which must be given in the proper irreducible tensorial form (La Penna et al., 1999b), are therefore bilinear and tetralinear, respectively, in the bond variables for 2-rank functions.

The autocorrelation functions accessed by Nuclear Magnetic Resonance experiments are of the form (Cavanagh et al., 1996):

$$\mathrm{TCF}(t) \;=\; \sum_{M=-2}^{2} \left\langle \left[D^{(2)*}_{M,0}(\Omega(t))/r^3(t) \right] \left[D^{(2)}_{M,0}(\Omega(0))/r^3(0) \right] \right\rangle \tag{20}$$

where $D^{(2)}_{M,0}$ are irreducible spherical tensors (Rose, 1957) and Ω and r are the direction and the modulus of the given H-H vector, respectively. A widely used approximation to the exact TCF is obtained by extracting r from the TCF:

$$\begin{aligned} \mathrm{TCF}(t) \;&\simeq\; \left\langle 1/r^6 \right\rangle \sum_{M=-2}^{2} \left\langle \left[D^{(2)*}_{M,0}(\Omega(t)) \right] \left[D^{(2)}_{M,0}(\Omega(0)) \right] \right\rangle \\ &=\; \left\langle 1/r^6 \right\rangle \langle P_2(\cos(\beta(t))) \rangle \end{aligned} \tag{21}$$

where P_2 is the Legendre polynomial of order 2 and β is the angle that the H-H vector spans in time t.

As f of Equation 10 is an L-rank irreducible spherical function of a molecular vector, the projections $\langle f|\phi_m\rangle$ on the basis elements ϕ_m are non-zero if and only if ϕ_m is an L-rank function. Therefore, the ϕ_m basis functions must be constructed as L-rank functions. As a consequence, the **S** and **F** matrix elements are averages of products of L-rank irreducible spherical tensors. The evaluation of these elements is done simply by computing the scalar components (rotational invariants) contained in the products of L-rank functions in the matrix elements (La Penna et al., 1999b; Fausti et al., 1999).

Summarizing, once a basis set of elements ϕ_m is given, the equilibrium averages estimated via MD are the rotational invariant of **S** and **F** matrix elements (Equations 14 and 15) and the rotational invariant of projections $\langle f|\psi_i\rangle$ (where f runs over each H-H vector distance included in the relaxation matrix, Equations 2–6. These latter projections are calculated through the projections $\langle f|\phi_m\rangle$ via Equation 12. Being the solution isotropic, the statistical averages are rotational invariants. Therefore, the global rotation occurring in the MD trajectory does not affect any result obtained by diffusion theory and the correlation functions of tensor variables approach asymptotically zero in the infinite time limit. The global rotational tumbling is contained in the diffusion equation, but is not assumed to be separated by any other relaxation mode in the macromolecule. The identification of rotational diffusion can be done only *a posteriori* by analysing the separation between the rates that are calculated using a given basis set and a given statistics.

We summarize below an efficient procedure for finding a reduced basis set so as to compute accurate tensor time correlation functions. The first step amounts to solve the diffusion equation with a basis that is linear in the bonds in order to get the first-order dynamics for a vector (1-rank) function:

$$\{l_{i,x}\}\; i = 1, \ldots, N_b. \tag{22}$$

The first-order solution is obtained by diagonalization of Equation 13, which gives the 1-rank first-order vector eigenfunctions $m_{i,x}$:

$$m_{i,\alpha} = \sum_{j=1}^{Nb} C_{j,i} l_{j,\alpha}. \tag{23}$$

For quasi-rigid structures, ignoring the modes of higher rates means neglecting very small contributions to the TCFs that correspond to fast decaying exponential terms related to these modes. This is evident to the first-order and is still valid to higher orders due to the combined effect of the products of fast decaying exponential terms. Therefore, we can select a reduced basis set, generally built with the e modes of Equation 23 of lowest rates, with e equal to the dimensionality d of the space or a value much lower than N_b.

For 2-rank functions, a reduced second-order basis set RM2-II (La Penna et al., 1999b) can be generated coupling the 1-rank first-order modes of Equation 23

in the proper irreducible tensorial form:

$$\begin{aligned}
\phi_{i1,i2,0} &= \tfrac{1}{2}(3m_{i1,z}m_{i2,z} - \mathbf{m}_{i1}\cdot\mathbf{m}_{i2}),\\
\phi_{i1,i2,-2} &= \sqrt{\tfrac{3}{8}}(m_{i1,x}m_{i2,x} - m_{i1,y}m_{i2,y}),\\
\phi_{i1,i2,+2} &= \sqrt{\tfrac{3}{8}}(m_{i1,x}m_{i2,y} + m_{i1,y}m_{i2,x}),\\
\phi_{i1,i2,-1} &= \sqrt{\tfrac{3}{8}}(m_{i1,x}m_{i2,z} + m_{i1,z}m_{i2,x}),\\
\phi_{i1,i2,+1} &= \sqrt{\tfrac{3}{8}}(m_{i1,y}m_{i2,z} + m_{i1,z}m_{i2,y}),\\
& i_1 = 1,\ldots,e; \quad i_1 \leqslant i_2.
\end{aligned} \tag{24}$$

where i_1 and i_2 run over the set of modes chosen among the 1-rank first-order solution of diffusion equation. This 2-rank first-order basis set is then expanded to second order adding the functions:

$$\begin{aligned}
\phi_{i1,i2,i3,i4,M} &= \phi_{i1,i2,M}(\mathbf{m}_{i3}\cdot\mathbf{m}_{i4})\\
& i_3 = 1,\ldots,e; \quad i_3 \leqslant i_4
\end{aligned} \tag{25}$$

Once e first-order vector modes are chosen, this second-order basis set contains $e(e+1)/2$ second powers (Equation 24) and $[e(e+1)/2]^2$ fourth powers (Equation 25) of the 1-rank first-order modes of Equation 23.

As observed in reference above, this second-order basis set RM2-II is expected to give a good approximation to the dynamics of fluctuating biological structures because it gives in the rigid limit the 'exact' rotational dynamics.

Once the 2-rank TCFs are generated, they can be Fourier transformed to the spectral densities

$$J(\omega) = 2\int_0^\infty \cos(\omega t)\ \mathrm{TCF}(t)\,\mathrm{d}t, \tag{26}$$

required to compute the relaxation matrix and the CP values in NOESY spectra via Equations 1–7.

Molecular dynamics simulations

A 10 ns molecular dynamics trajectory was calculated with the AMBER 5.0 program (Pearlman et al., 1995) as described elsewhere (Kieken et al., in preparation). It was obtained in the presence of 22 counterions and 4313 explicit water molecules at 300 K in the NPT ensemble using the particle-mesh Ewald algorithm (Darden et al., 1993) for evaluating electrostatic forces. The NMR structure of the stem-loop (Kieken et al., in preparation) was used as the initial configuration and the energy was minimized with 100 steps of steepest descent algorithm followed by 900 conjugate gradient steps. Thermalization in the presence of water and counterions was performed in two stages. In the first stage only water was allowed to move (BELLY option of AMBER) and successive 2 ps runs at temperatures ranging from 50 K to 300 K by steps of 50 K were performed with reassigning atomic velocities every 0.5 ps. The second heating stage was identical to the first one with the exception that all atoms were free to move. This was followed by 200 ps simulation at 300 K for further equilibration. During the production period, atomic coordinates were stored every 0.5 ps leading to a total of 20 000 configurations to be analyzed. The time increment for solving Newton equations was 2 fs and the SHAKE algorithm was used on all the covalent bonds (Ryckaert et al., 1977). Along the trajectory, the root mean square fluctuation of the kinetic energy was less than 0.5% of the total kinetic energy.

Modeling the cross-peaks by diffusion theory coupled to MD simulations

The first test to perform is the dependence of the calculated CPs on the choice of the beads in the polymer model. The basic model (model B hereafter) has two groups in the backbone: one is centered in P (grouping the phosphate and the methylene 5′) and the other in C4′ (grouping the ribose ring atoms). Pyrimidine bases are represented by only one bead centered in N1, while purine bases are divided into two beads one centered in N9 (grouping imidazole ring atoms) and the other in N1 (grouping the remaining atoms of the base) (see Table 1). The 5′ end is the group HO-CH_2 centered in O5′; for the 3′ end, the terminal OH is added to the ribose bead. This first choice is motivated by the good modeling obtained in previous studies on DNA fragments (Fausti et al., 1999; La Penna et al., 2000b). Nevertheless, two other models have been considered (Table 1). The first model (model B5) separates the methylene group centered in C5′ from the phosphate bead: this was motivated by indications of differential mobilities in nucleic acids in previous studies (Briki and Genest, 1995; Bruant et al., 1999). The second model (model BH) differs from model B by separating atom H6 for pyrimidine and H8 for purine from the bead centered in N1 to better describe a system of interacting hydrogens as that probed by NOESY experiments.

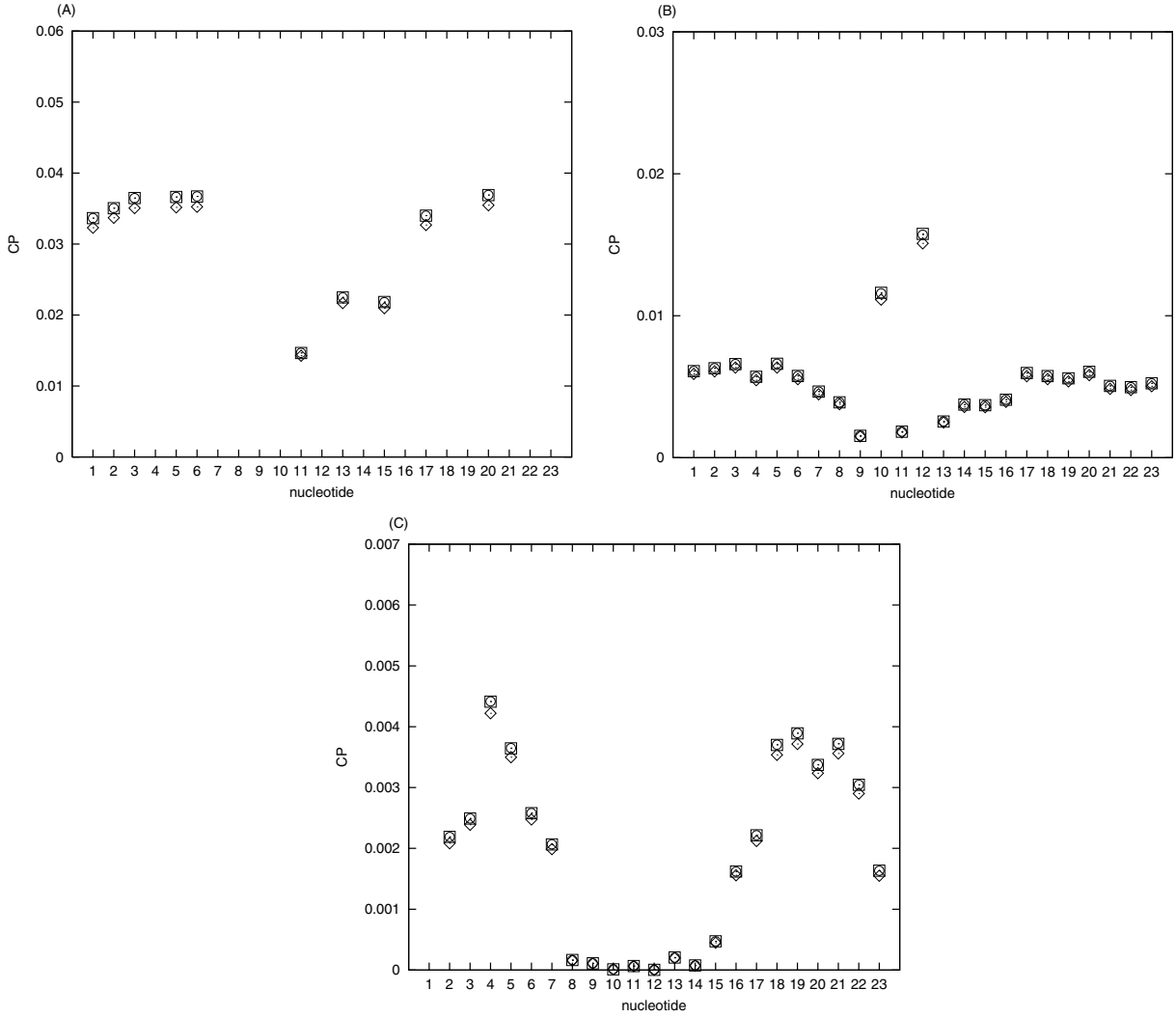

Figure 1. NOESY cross-peak intensities (CP) for different H-H pairs in each nucleotide for different bead models in the diffusive approach: H5(i)-H6(i) *intra* at 50 ms mixing time (A); H1′(i)-H6/8(i) *intra* (B) and H1′(i−1)-H6/8(i) *inter* (C) at 100 ms mixing time. Model B (squares); model B5 (diamonds); model BH (circles).

For the comparison of the performance of different bead models, the diffusion calculations of the CPs at $\nu = 500$ MHz were performed using the reduced basis set RM2-II with $e = 3$. The mixing time delay was set to 50 ms for H5-H6 *intra* pairs and 100 ms for H1′-H6/8 pairs, respectively, to be consistent with further calculations and comparisons with experiments. Figure 1 shows that the effect of the bead model is overall very small, models B and BH giving almost coinciding results, just showing that it is not necessary to consider explicitly the hydrogens, from a hydrodynamic point of view; model B5 displays a modest difference which is related to the separation of C5′ from the phosphate (Bruant et al., 1999). In consideration of these results, in the following comparisons and discussions we adopt only the simpler model B.

Is there any effect of the number of first order vector modes e in the second order diffusion calculations? Figure 2 shows that computations with $e = 4$ or 5 in respect to the case $e = 3$ does not give important additional contributions to the CPs. Effects, even though small, are visible only in the loop as is reasonable, since the loop is more flexible than the stem. That is to say, according to the statistics used here, the modes of high rate describe fast decaying fluctuations of small importance for the CP intensities at the chosen

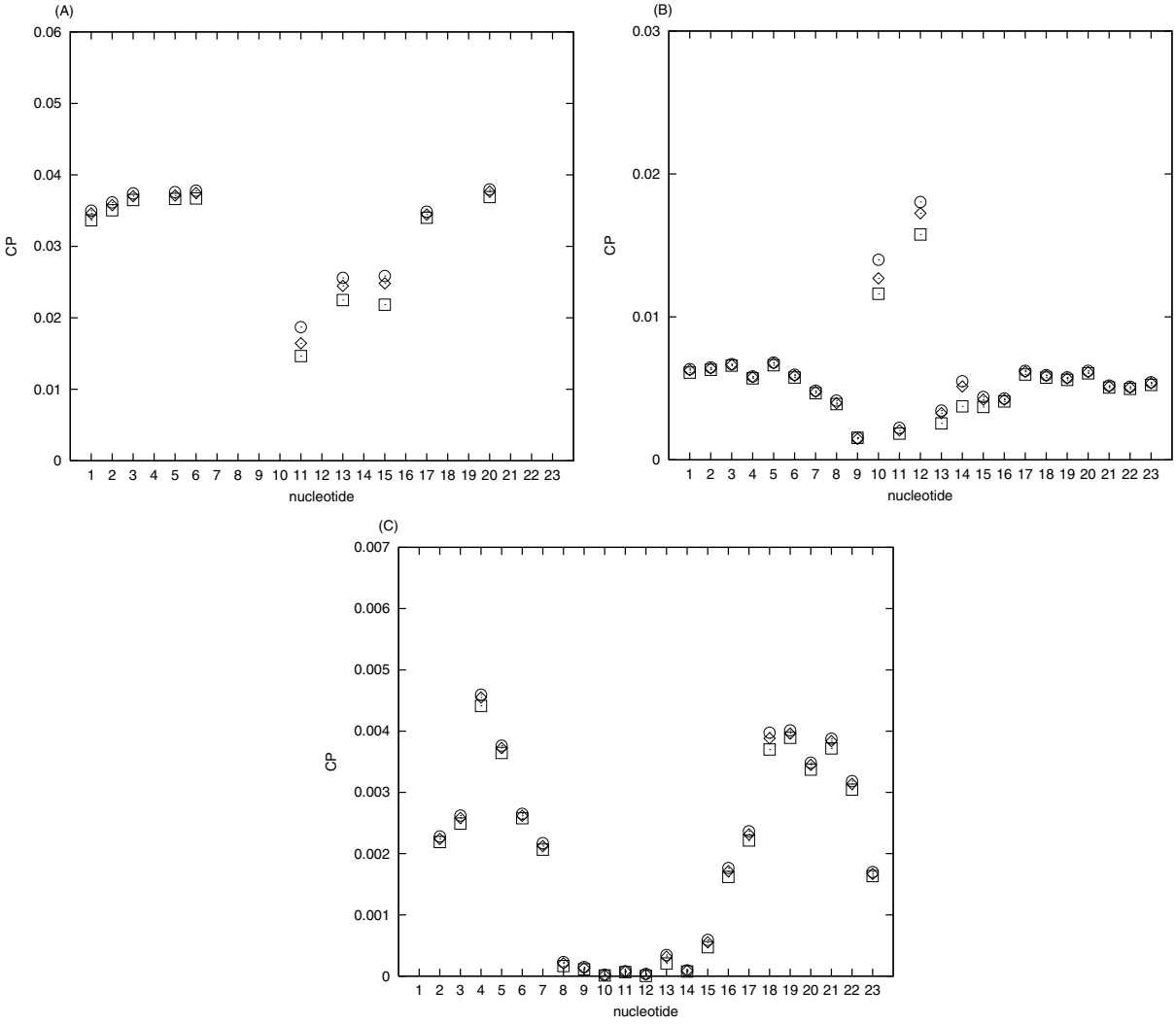

Figure 2. NOESY cross-peak intensities (CP) for different H-H pairs in each nucleotide for bead model B using different basis sets in the diffusive approach: H5(i)-H6(i) *intra* at 50 ms mixing time (A); H1′(i)-H6/8(i) *intra* (B) and H1′(i−1)-H6/8(i) *inter* (C) at 100 ms mixing time. Mode-coupling approximation with $e = 3$ (squares); $e = 4$ (diamonds); $e = 5$ (circles).

mixing times. Therefore we decide to perform further computations using $e = 3$ to save computing time.

In Figures 3A–C we analyze the dependence of the CP patterns on the length of the trajectory in the three cases of H5-H6 *intra*, H1′-H6/8 *intra*, H1′-H6/8 *inter* pairs. First, the effect of flexibility on the CPs values must be noticed that is particularly evident for H5-H6 *intra* pairs (Figure 3A), where the H5-H6 distance r is almost constant (see later comments to Figure 4A). In the case of the starting rigid structure, the variation of CPs in Figure 3A is mainly due to the factor r^{-6} where r ranges from 0.23 to 0.26 nm. But this variation is spread over all the C/U residues representing the effect on CPs of a configuration where the inter-proton distances are thermally distributed. On the other hand, CPs resulting from the statistical averages for the fluctuating structure are clearly separated in two domains, the stem (residues 1, 2, 3, 5, 6, 17 and 20) and the loop (residues 11, 13 and 15): there is no evidence both in X-ray crystallography and in NMR that a significant change of C/U base ring average interatomic distances occurs with stacking or hydrogen bonding of bases. In the following analysis, the correlation between H5-H6 *intra* CPs and the orientational mobility of the H5-H6 unit vector will be shown.

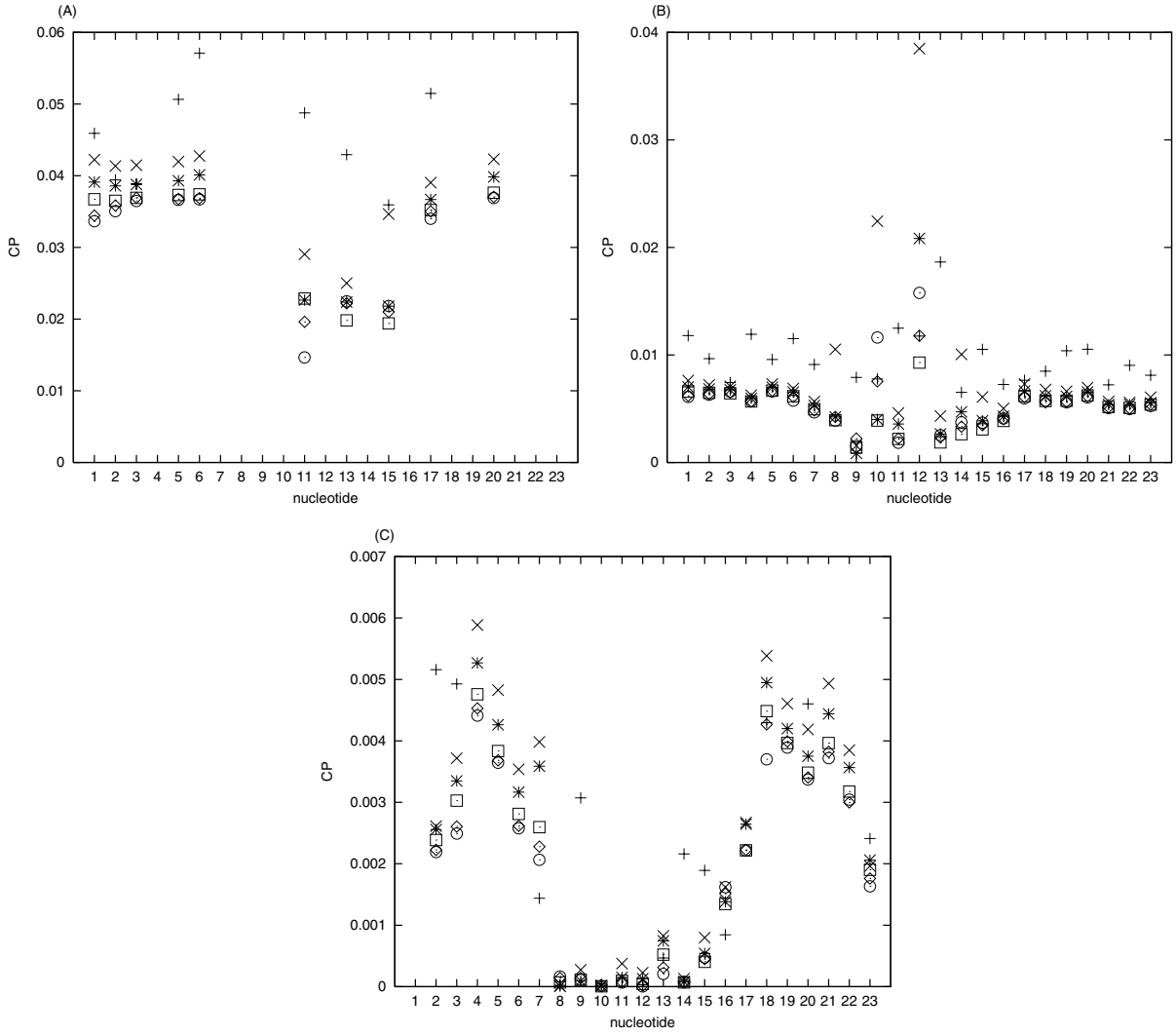

Figure 3. NOESY cross-peak intensities (CP) for different H-H pairs in each nucleotide for bead model B with $e = 3$ for different MD trajectory lengths: H5(i)-H6(i) *intra* at 50 ms mixing time (A); H1′(i)-H6/8(i) *intra* (B) and H1′(i−1)-H6/8(i) *inter* (C) at 100 ms mixing time. Rigid starting structure (plus); trajectory of 2 ns (crosses); 4 ns (asterisks); 6 ns (squares); 8 ns (diamonds); 10 ns (circles). Some of the data for the rigid structure are out of range in the y axis and are not displayed to emphasize the behaviour of the other data.

After the trajectory has reached the length of 6 ns, it can be seen from all three plots in Figure 3 that the effects of the statistics on the calculated CPs are in general modest. In the case of H5-H6 *intra*, the only exception is nucleotide C11, where a clear reduction of the CP is produced by adding the last two nanoseconds of the trajectory. As observed elsewhere (Kieken et al., in preparation), this effect is related to an evident change in the structure of the RNA fragment occurring during the third quarter of the trajectory, when base C11 is pushed outside of the loop, while bases G10 and A12 are directed inward. Significant variations of CPs along with the trajectory length can be observed in Figure 3B for residues 10 and 12 that are affected by the same conformational change. Figure 3C shows that the convergence of computed CPs with the trajectory length is not achieved. A discussion on the specific case of H1′-H6/8 *inter* CPs will be presented later in the frame of the effects of relaxation pathways. The above comments about figures 3A and 3B do not change the possible conclusions of the comparisons with the experiments given the errors in both the calculations and experiments. Nevertheless, it is a warning on the fact that the statistics we use may badly describe

slow fluctuations on the scale of several nanoseconds, which in turn may affect the real statistics. This is a general problem to consider when dealing with these types of computations.

Comparison with NOESY experiments

Before comparing MCD calculations and NMR data, we focus on the fact that the most reliable CPs are those measured at the short mixing time of 50 ms for H5-H6 *intra* pairs, atoms which are very close at an almost constant distance (0.244 ± 0.008 nm). For these reasons the estimated errors are not so large so as to question the general differential trends for the stem and the loop and it is expected that the computation of the CP does not require the knowledge of the inter-proton distance variation. In Figure 4A, the experimental values show the different behavior between the two domains in the molecule: the CPs in the stem are higher than those in the loop and have similar values in the two strands which indicates the larger mobility of the loop. A doubt could arise about nucleotide C20, whose value is slightly lower than the average value of the CPs in the stem but still higher than those in the loop. These important differences between stem and loop are well highlighted by the calculations, where the separation between the behavior of the loop and the two strands of the stem is even more evident. As regards the calculations, the CP in nucleotide C11 is slightly lower than the average of the other CPs in the loop (and in addition compared to its corresponding experimental value). In this case, this behavior could be due to an artifact in the statistics. The general features of Figure 4B are similar, but with the noteworthy difference that in the loop region there is a larger dispersion of the points both in experiments and calculations (even though differently located) which indicates an even larger disorder or mobility in the loop for H1′-H6/8 *intra* CPs. In addition, we must also take note that the high calculated values at nucleotides G10, A12 are due to the MD statistics, as discussed below. In the case of H1′-H6/8 *inter* CPs (Figure 4C), despite the high dispersion of both theoretical and experimental points, we can see again, on average, lower values in the loop well matched by the calculations. These general similarities will be better understood after viewing the analysis and discussions of the following section.

Understanding the differential mobility of the RNA fragment and discussion

What can we deduce by the MCD calculations on the important mobility effects in the RNA fragment?

A first point which can be addressed is an analysis of the most relevant contributions to the full relaxation matrix that are responsible of the NOESY spectrum. While the above calculations were performed using the full relaxation matrix including all the 252 hydrogens in the molecule (*full* CPs), now we consider also the CPs calculated by reducing the number of the interacting hydrogens. For each H5-H6 or H1′-H6/8 pair the CP has been evaluated defining an isolated spin-system that contains only the hydrogen atoms within a distance of 0.6 nm from each of the two observed protons (hereafter indicated as *reduced* CPs). In addition, we have considered the CP values arising only from the direct dipolar coupling of the two observed hydrogens (*single* CPs) (see Equation 8). Figures 5A and 5B show that the calculated *reduced* CPs almost coincide with the *full* ones, while the *single* values are only slightly higher. This indicates that for H5-H6 and H1′-H6/8 *intra* CPs the contribution of the hydrogens located further than 0.6 nm from the observed atoms is negligible at these mixing times and the direct coupling between spins accounts for the largest contribution. Different is the case of Figure 5C which involves H1′-H6/8 *inter* CPs of contiguous nucleotides, characterized by larger distances than in the case of the previous *intra* CPs. In the case of the loop CPs a differentiation of the contributions has a limited meaning due to the very small CP values and will be not pursued here. On the contrary, on the two strands of the stem, while *full* and *reduced* CP calculations are almost coincident as in Figures 5A and 5B, the *single* CPs are very similar for the two strands and ignore the dispersion of the *full* calculation and of the experimental data. At this point it is appropriate to observe that the *single* H1′-H6/8 *inter* CPs, unlike *full* and *reduced* CPs, show a good convergence along with the trajectory length (calculations not shown). The *single* calculation gives a direct reliable description of the relaxation of the H1′-H6/8 distance and for this reason is a better index of the molecule's local mobility. Looking at the *single* calculations, the three cases are much more similar even though they are related to different distances and have such different magnitudes. From Equation 8, at short mixing times, one derives that the *single* CPs are proportional to the correlation times, τ, of the 2-rank TCF relative to the distance

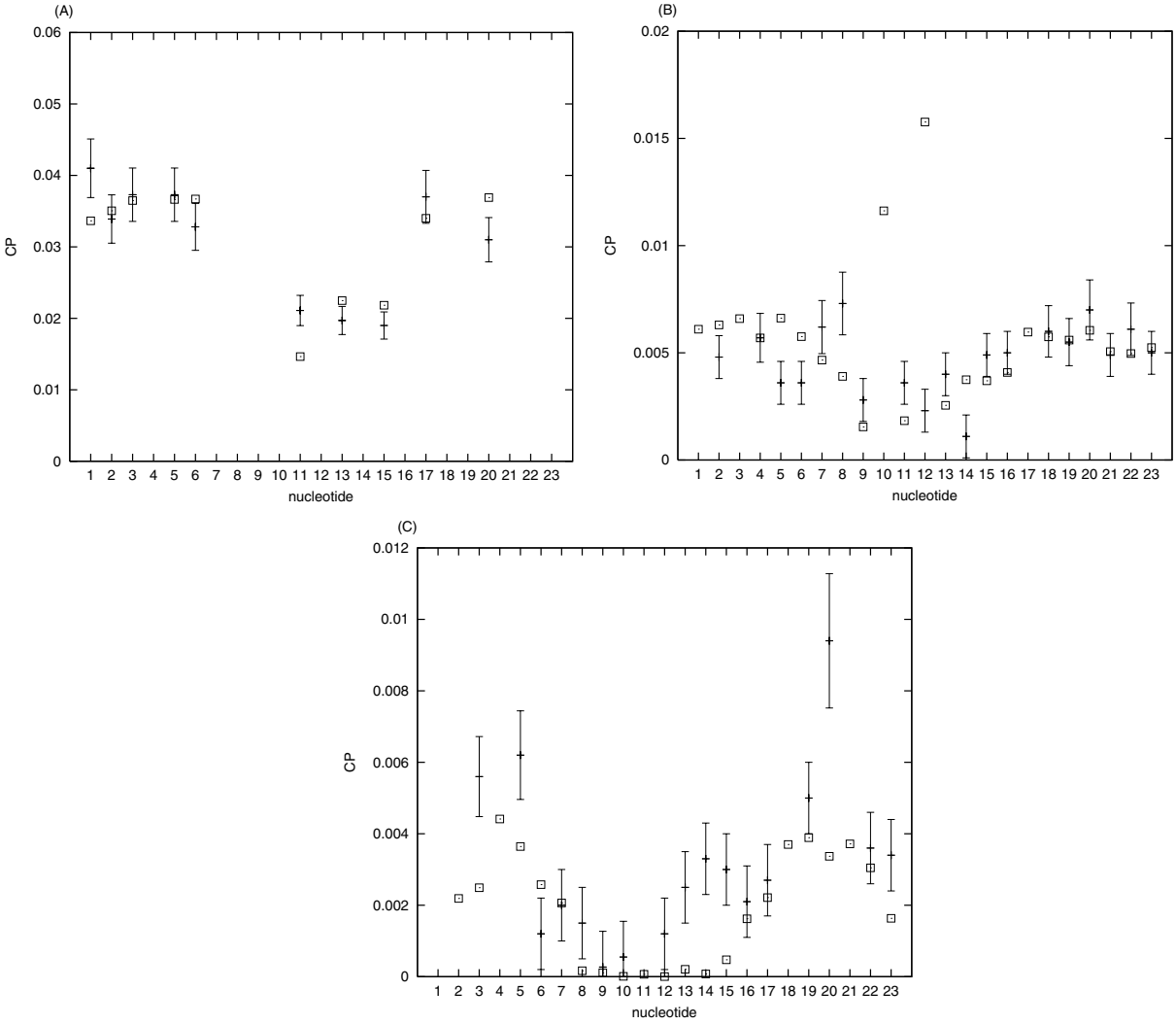

Figure 4. Comparison between calculated and experimental NOESY cross-peak intensities (CP) for different H-H pairs in each nucleotide. Calculations for bead model B with $e = 3$ and MD trajectory of 10 ns (squares); experimental data (points with error bars). Pairs H5(i)-H6(i) *intra* at 50 ms mixing time (A); H1′(i)-H6/8(i) *intra* (B) and H1′(i−1)-H6/8(i) *inter* (C) at 100 ms mixing time.

vectors of the observed pairs. The *single* CPs are more sensitive to the local dynamics of the observed pair of hydrogens than the *full* CPs, because the latter CPs are the complicated result of relaxing processes of many distances, due to spin diffusion.

In order to separate the effects of the distances and of the orientational fluctuations on the *single* CPs, we report in Figures 6A–C the comparison between the correlation times, τ, of the function observed in NMR and those of $P_2(t)$, τ_o . According to the discussion in reference Fausti et al. (1999) the sum of two exponential functions is a close approximation to the $P_2(t)$ TCF. The first exponential function, associated to overall rotational diffusion, has an amplitude that is an order parameter. For this molecule we observed that the order parameter displays the same behavior as τ_o (results not shown). Therefore, the behavior of the latter correlation time in the three patterns reflects only the order in the two strands of the stem compared to the disorder of the loop. The correlation time τ displays, with respect to τ_o, the further effects of the H-H distances. It is now clear that part of the behavior of the *single* CPs is related not only to the relaxation of the 2-rank spherical tensor, but also to the variation of the H-H distances along the sequence. In the case of the almost constant distances for H5-H6 CPs, these

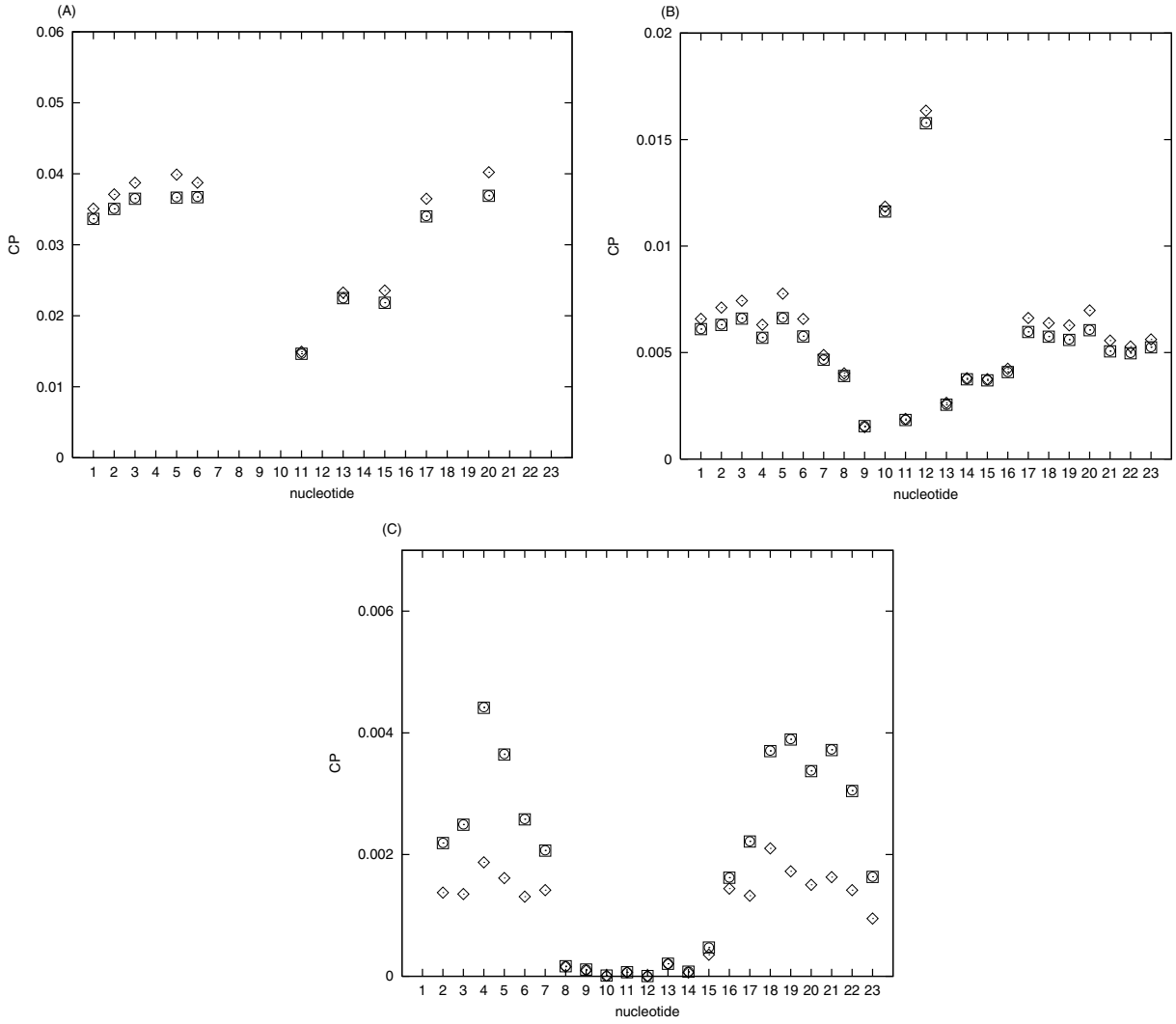

Figure 5. NOESY cross-peak intensities (CP) for different H-H pairs in each nucleotide for bead model B with $e = 3$ for the MD trajectory of 10 ns computed with different relaxation matrices: H5(i)-H6(i) *intra* at 50 ms mixing time (A); H1′(i)-H6/8(i) *intra* (B) and H1′(i−1)-H6/8(i) *inter* (C) at 100 ms mixing time. Full relaxation matrix (*full* calculation, squares); all the protons within 0.6 nm from each member in the observed pair (*reduced* calculation, circles); 2×2 matrix with only the two observed protons (*single* calculation, diamonds).

variations have no detectable effect, while they affect significantly H1′-H6/8 CPs. For instance, nucleotides 10 and 12 show the shortest average distances between H1′ and H8 atoms: this produces large H1′-H8 *intra* CPs, both for *single* and *full* calculations. In turn, the correlation times for the corresponding unit vectors τ_o do not show larger values for nucleotides 10 and 12 (see comparison between τ and τ_o in Figure 6B). Going back to Figure 4B, where the calculations are compared to the data, we notice that, giving the sensitivity of *intra* CPs to H-H distances shown above, experiments for A12 do not display such a short distance. Therefore, the short calculated distance could be due either to the confinement of the structure in a local minimum or to a deficiency in the force-field. On the other hand, Figure 6C shows that the large distances involved in the H1′-H6/8 *inter* pairs flatten the significant variation of τ_o in the loop (C11, G14 and C15).

Finally, we explain the large residual difference between the *single* and the *full inter* CPs of Figure 5C. The large increase of the CPs in the *full* pattern is a clear evidence of the importance of the non direct H-H interactions. In fact, in this particular case the

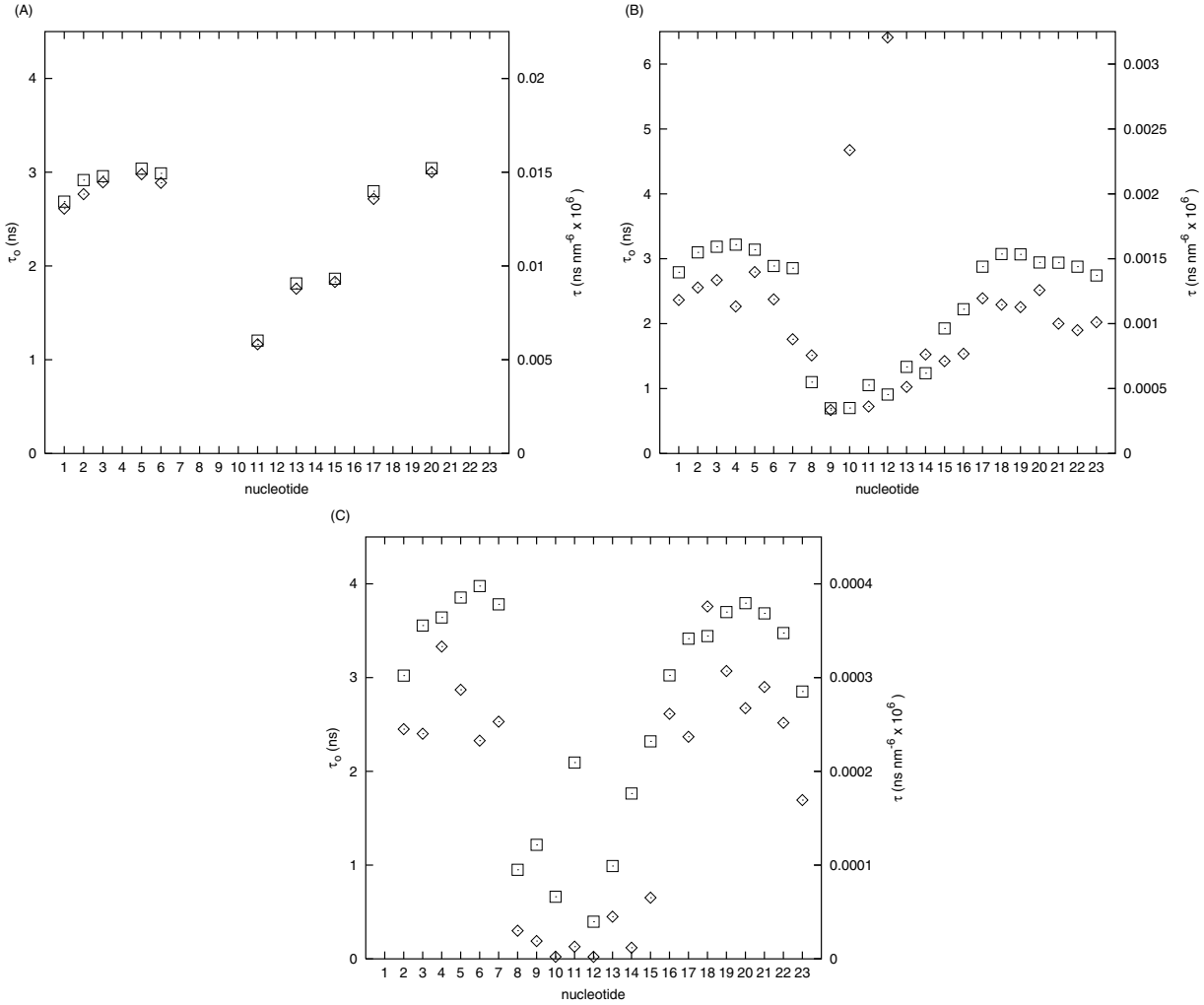

Figure 6. Comparison between calculated correlation times for different H-H pairs in each nucleotide for bead model B with $e = 3$ and MD trajectory of 10 ns. Exact time correlation function (Equation 20 in the text, diamonds and right y axis); orientational time correlation function (Equation 21 in the text, squares and left y axis). Pairs H5(i)-H6(i) *intra* (A); H1′(i)-H6/8(i) *intra* (B) and H1′(i−1)-H6/8(i) *inter* (C).

observed hydrogens are so far apart that the magnetization transfer is enriched by interactions with other closer hydrogens. For instance, the H1′(i)-H2′(i) and H6/8(i+1)-H2′(i) distances are around 0.22 nm as opposed to the long H1′(i)-H6/8(i+1) distance (about 0.5 nm). Note that for DNA, also the *intra* case displays spin-diffusion effects due to the presence of H2″ that substitutes the 2′ hydroxyl (Gaudin et al., 1995).

What is the effect of the fluctuations of the H-H distances on the CPs?

In Figure 7B and B the *full* CPs calculated from the second rank TCF relative to the distance vectors of the pairs, Equation 20, and from the second rank orientational TCF with averaged $1/r^6$, Equation 21, are compared. Negligible effects are found in the case of H5-H6 *intra* (results not shown) because the only important distance is the stiff H5-H6 distance. In the H1′-H6/8 *intra* case, the contributions are significant mainly in the loop and at the border of the stem, where the fluctuations are more relevant. In the *inter* case the effect of fluctuations on these large distances is observed along the whole sequence both in the loop and in the stem. In any case, the contribution of distance fluctuations is modest and cannot affect the main conclusions of the calculations.

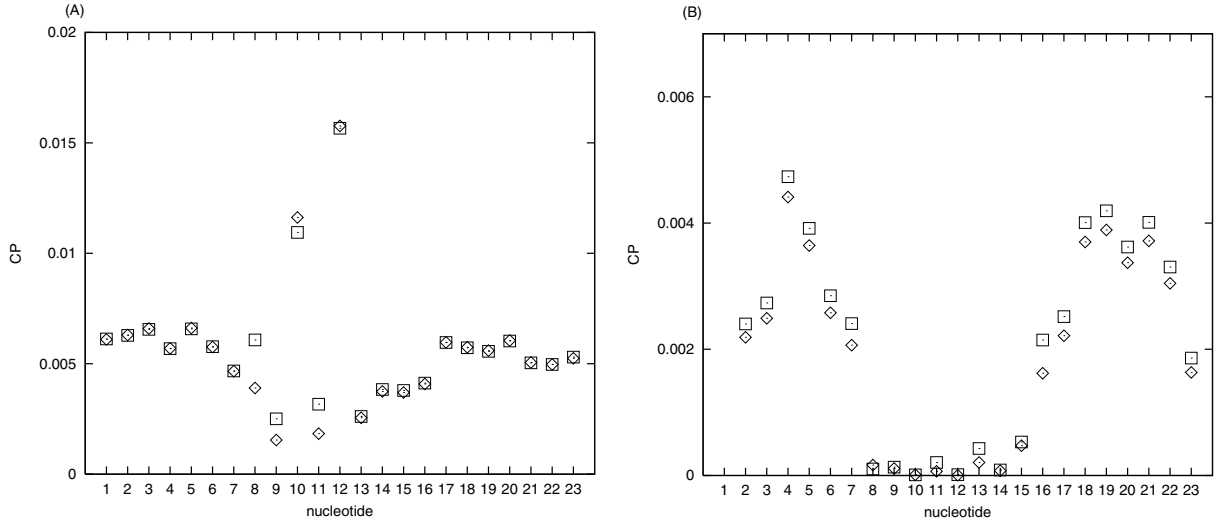

Figure 7. NOESY cross-peak intensities (CP) for different H-H pairs in each nucleotide for bead model B with $e = 3$ for the MD trajectory of 10 ns computed with the two time correlation functions defined in the text: exact time correlation function (Equation 20 in the text, diamonds); orientational time correlation function (Equation 21 in the text, squares). Pairs H1′(i)-H6/8(i) *intra* (A) and H1′(i−1)-H6/8(i) *inter* (B).

Conclusions

The diffusive dynamics of the mutated stem-loop SL1 domain in the HIV-1_{Lai} genome has been described within the mode-coupling approximation. This RNA domain has a key role in the dimerization of the HIV-RNA and is characterized by a structured double helix stem and a flexible loop of nine nucleotides. The diffusive approach enables both a detailed understanding of the NOESY NMR relaxation data and an atomistic description of the dynamics.

In particular, the ^{1}H-NOESY data related to close hydrogens, like the H5-H6 pairs in pyrimidines, can be considered as probes for monitoring local dynamics along the sequence: these H5-H6 *intra* cross-peaks are characterized by significant and reliable intensities at low mixing times, with minimal experimental errors. The low mixing time allows the neglecting of relaxation mechanisms (like the transfer of excitation to the environment) that become significant as mixing time increases and difficult to model in the relaxation matrix. The diffusion approach, applied to these data enables a quantitative analysis of the differential mobilities in the stem and loop, confirming the high disorder of the loop. Again, it must be remarked that this quantitative comparison can be performed using ^{1}H-NOESY maps that do not require expensive and time-consuming sample enrichment.

In the case of hydrogen pairs located at far distance in space, the agreement with experiments is only qualitative. Nevertheless, the diffusive analysis helps in the separation of different contributions to the CPs: the orientational mobility of the observed H-H unit vector; the effect of the observed H-H distance both fluctuating and in the average; finally, the effect of relaxation pathways alternative to the direct one. In the case of H5-H6, only the first process is important due to the short and stiff distance involved. For H1′-H6/8 *intra* CPs we demonstrated the importance of the average distances in modulating the effect of the orientational mobility. Because of the large sensitivity of CPs at larger mixing times to correct estimates of the average distances between protons, it is clear and well known that these data are best suited for structure determination.

Finally, for *inter* CPs only, alternative relaxation pathways become important especially in the stem. Inclusion of H-H distance fluctuations in the TCF introduce minor effects which can be observed mainly in the loop for H1′-H6/8 CPs.

Globally, the main general conclusion is that an accurate analysis is necessary to extract from the cross-peak data the real local mobility. We have shown that this analysis may be provided by using the diffusive approach and that short mixing time CPs relative to proton pairs that are close in space can be used as good measures of mobility provided the CPs can be easily obtained and are reliable. In this respect, the analysis of such CPs can be a valid alternative to measurements of ^{13}C or ^{15}N nuclear magnetic relaxation parameters

in enriched samples, thus reducing significantly the efforts to obtain information about the macromolecular mobility. Even if analysis of ^{1}H-NOE build-up rates are reported in the literature by using MD simulations and several diffusive approximations (Whitka et al., 1991), this is the first time that ^{1}H-NOESY CPs are shown to contain reliable information about molecular mobility that can be quantitatively interpreted within diffusion theory. The level of diffusion theory applied in this paper does not preclude the manifestation of mixed modes in the correlation functions because it does not assume separation between time-scales in the molecular dynamics. Rather, an *a posteriori* analysis of the results allows the identification of the essential relaxation modes that describe the experiments.

As regards the modeling of the diffusion approach, the addition of more beads to the standard model, including three or four beads in the bases for pyrimidines or purines, respectively, gives only modest contributions. In the construction of higher order basis sets, the consideration of only three 1-rank first-order rotational modes is a sufficiently good approximation. Note that this does not mean that only rotational diffusion is assumed because even these lower-rate modes are affected by the fluctuations of the structure. This set-up, due to its simplicity, can be extended to larger molecules.

The major limitation of the method consists in the approximation to the conformational statistics, which is here evaluated by time averaging along a molecular dynamics trajectory, though the trajectory used in this work is very long (10 ns) in terms of computational time. It can be pointed out that for our 23-nucleotide stem-loop, this trajectory is sufficient to well compute most of the CPs. This occurs even in the case of *intra* CPs with fluctuating interproton distances and of *inter* CPs where the distances between the observed hydrogens are large, fluctuating and the spin diffusion plays a significant role at 100 ms mixing time. Nevertheless, trapping in a local minimum, defects on the empirical force-field and insufficient trajectory length are the main origins of discrepancies between theory and experiment. Any simulation technique able to overtake such problems while keeping the essential features of the force-field affecting biopolymer stability will greatly enhance the quality of diffusion theory results.

Acknowledgements

This work has been done within the IMAG-CNR/CBM-CNRS cooperation project 'Coupling of analytical methods and numerical simulations in the study of internal molecular dynamics in the SL1 domain dimerization of HIV-1 genomic RNA' 2000-2001.

References

Boelens, R., Koning, T.M.G., Van der Marel, G.A., Van Boom, J.H. and Kaptein, R. (1989) *J. Magn. Reson.*, **82**, 290–308.

Briki, F. and Genest, D. (1995) *J. Biomol. Struct. Dyn.*, **12**, 1063–1082.

Bruant, N., Flatters, D., Lavery, R. and Genest, D. (1999) *Biophys. J.*, **77**, 2366–2376.

Cavanagh, J., Fairbrother, W.J., Palmer III, A.G. and Skelton, N.J. (1996) *Protein NMR Spectroscopy*, Academic Press, San Diego, CA, pp. 243–300.

Clore, G.M., Szabo, A., Bax, A., Kay, L.A., Driscoll, P.C. and Gronenborn, A.M. (1990) *J. Am. Chem. Soc.*, **112**, 4989–4991.

Darden, T.A., York, D.M. and Pedersen, L.G. (1993) *J. Chem. Phys.*, **98**, 10089–10092.

Fausti, S., La Penna, G., Cuniberti, C. and Perico, A. (1999) *Biopolymers*, **50**, 613–629.

Fausti, S., La Penna, G., Cuniberti, C. and Perico, A. (2000) *Mol. Simul.*, **24**, 307–324.

Forster, M.J. (1991) *J. Comput. Chem.*, **12**, 292–300.

Gaudin. F., Paquet, F., Chanteloup, L., Beau, J.-M., Thuong, N.T. and Lancelot, G. (1995) *J. Biomol. NMR*, **5**, 49–58.

Girard, P.-M., Bonnet-Mathonière, B., Muriaux, D. and Paoletti, J. (1995) *Biochemistry*, **34**, 9785–9794.

Girard, F., Barbault, F., Gouyette, C., Huynh-Dinh, T., Paoletti, J. and Lancelot, G. (1999) *J. Biomol. Struct. Dyn.*, **16**, 1145–1157.

Jeener, J., Meier, B.H., Bachmann, P. and Ernst, R.R. (1979) *J. Chem. Phys.*, **71**, 4546–4553.

La Penna, G., Mormino, M., Pioli, F., Perico, A., Fioravanti, R., Gruschus, J.M. and Ferretti, J.A. (1999a) *Biopolymers*, **49**, 235–254.

La Penna, G., Pratolongo, R. and Perico, A. (1999b) *Macromolecules*, **32**, 506–513.

La Penna, G., Fausti, S., Perico, A. and Ferretti, J.A. (2000) *Biopolymers*, **54**, 89–103.

La Penna, G., Perico, A. and Genest, D. (2000) *J. Biomol. Struct. Dyn.*, **17**, 673–685.

Laughrea, M. and Jetté, L. (1994) *Biochemistry*, **33**, 13464–13474.

Lipari, G. and Szabo, A. (1982) *J. Am. Chem. Soc.*, **104**, 4546–4570.

Macura, S. and Ernst, R.R. (1980) *Mol. Phys.*, **41**, 95–117.

Marquet, R., Paillart, J.-C., Skripkin, E., Ehresmann, C. and Ehresmann, B. (1994) *Nucleic Acid Res.*, **22**, 145–151.

Meier, B.H. and Ernst, R.R. (1979) *J. Am. Chem. Soc.*, **101**, 6441–6442.

Mujeeb, A., Clever, J.L., Billeci, T.M., James, T.L. and Parslow, T.G. (1998) *Nat. Struct. Biol.*, **5**, 432–436.

Muriaux, D., Girard, P.-M., Bonnet-Mathonière, B. and Paoletti, J. (1995) *J. Biol. Chem.*, **270**, 8209–8216.

Muriaux, D., De Rocquigny, H., Roques, B. and Paoletti, J. (1996) *J. Biol. Chem.*, **271**, 33686–33692.

Neuhaus, D. and Williamson, M. (1989) *The Nuclear Overhauser Effect in Structural and Conformational Analysis*, VCH Publishers Inc., New York, NY.

Pastor, R.W. and Karplus, M. (1988) *J. Phys. Chem.*, **92**, 2636–2641.

Pearlman, D.A., Case, D.A., Caldwell, G.W., Ross, W.S., Cheatman, T.E., Ferguson, D.M., Seibel, G.L., Singh, U.C., Weiner, P.K. and Kollman, P.A. (1995) AMBER 5.0, University of California at San Francisco, San Francisco, CA.

Paillart, J.-C., Marquet, R., Skripkin, E., Ehresmann, B. and Ehresmann, C. (1994) *J. Biol. Chem.*, **269**, 27486–27493.

Perico, A. and Pratolongo, R. (1997) *Macromolecules*, **30**, 5958–5969.

Prompers, J.J. and Brüschweiler, R. (2000) *J. Phys. Chem. B*, **104**, 11416–11424.

Prompers, J.J., Scheurer, C. and Brüschweiler, R. (2001) *J. Mol. Biol.*, **305**, 1085–1097.

Rose, M.E. (1957) *Elementary Theory of Angular Momentum*, John Wiley & Sons, New York, NY.

Ryckaert, J.P., Cicotti, G. and Berendsen, H.J.C. (1977) *J. Comput. Phys.*, **23**, 327–341.

Sanders, J.K.M. and Hunter, B.K. (1993) *Modern NMR Spectroscopy*, Oxford University Press, Oxford, UK.

Skripkin, E., Paillart, J.-C., Marquet, R., Ehresmann, B. and Ehresmann, C. (1994) *Proc. Natl. Acad. Sci. USA*, **91**, 4945–4949.

Solomon, I. (1955) *Phys. Rev.*, **99**, 559–565.

Theilleux-Delalande, V., Girard, F., Huynh-Dinh, T., Lancelto, G. and Paoletti, J. (2000) *Eur. J. Biochem.*, **267**, 2711–2719.

Tugarinov, V., Liang, Z., Shapiro, Y.E., Freed, J.H. and Meirovitch, E. (2001) *J. Am. Chem. Soc.*, **123**, 3055–3063.

Withka, J.M., Swaminathan, S., Beveridge, D.L. and Bolton, P.H. (1991) *J. Am. Chem. Soc.*, **113**, 5041–5049.

Wüthrich, K. (1986) *NMR of Proteins and Nucleic Acids*, Wiley, New York, NY.